Chapter I : Theoretical background

As it was presented in the introduction, the subject of this thesis is the study of the phase transformations and mechanical properties of stainless and other highly alloyed steel grades. The phase transformations and the mechanical properties are closely related through the TRIP effect (transformation-induced plasticity). Indeed, during straining, the metastable austenite transforms into martensite, enhancing the ductility and the resistance. The transformations are governed by two parameters : the thermodynamic relative stability of the different phases which depends on the chemical composition and the temperature ; and the stacking fault energy that controls the crystallographic mechanisms of plastic deformation. This Chapter will thus briefly present the different factors that affect the phase stability and the stacking fault energy. The phenomena related to the plastic deformation will be summarised under the light of these two parameters and the crystallographic mechanisms of phase transformation will be developed.

I.1 Phase Stability

I.1.1 Phases and crystal lattices

Iron alloys present a large variety of phases and Bravais lattices :

- austenite : face-centered cubic (FCC) ;
- ferrite : body-centered cubic (BCC) ;
- ε phase : hexagonal close-packed (HCP) ;
- …

The BCC structure (body centred cubic), which is not a close-packed structure, has a coordination number of 8. The FCC and HCP structures are close-packed structures with a coordination number of 12. Figure I.1 illustrates how the FCC and HCP structures can be built up based on the stacking of close-packed planes (CPP). Starting from a first plane named A, two positions (B or C) are possible for the atoms of the neighbour CPP as shown by Figure I.1 (b). In the same way, over the plane B, the next CPP can be either in A or C positions as shown on Figure I.1 (c). Two stable stackings can then be formed : …ABABABAB… brings about a HCP structure while the FCC structure results from a …ABCABCABC… stacking.

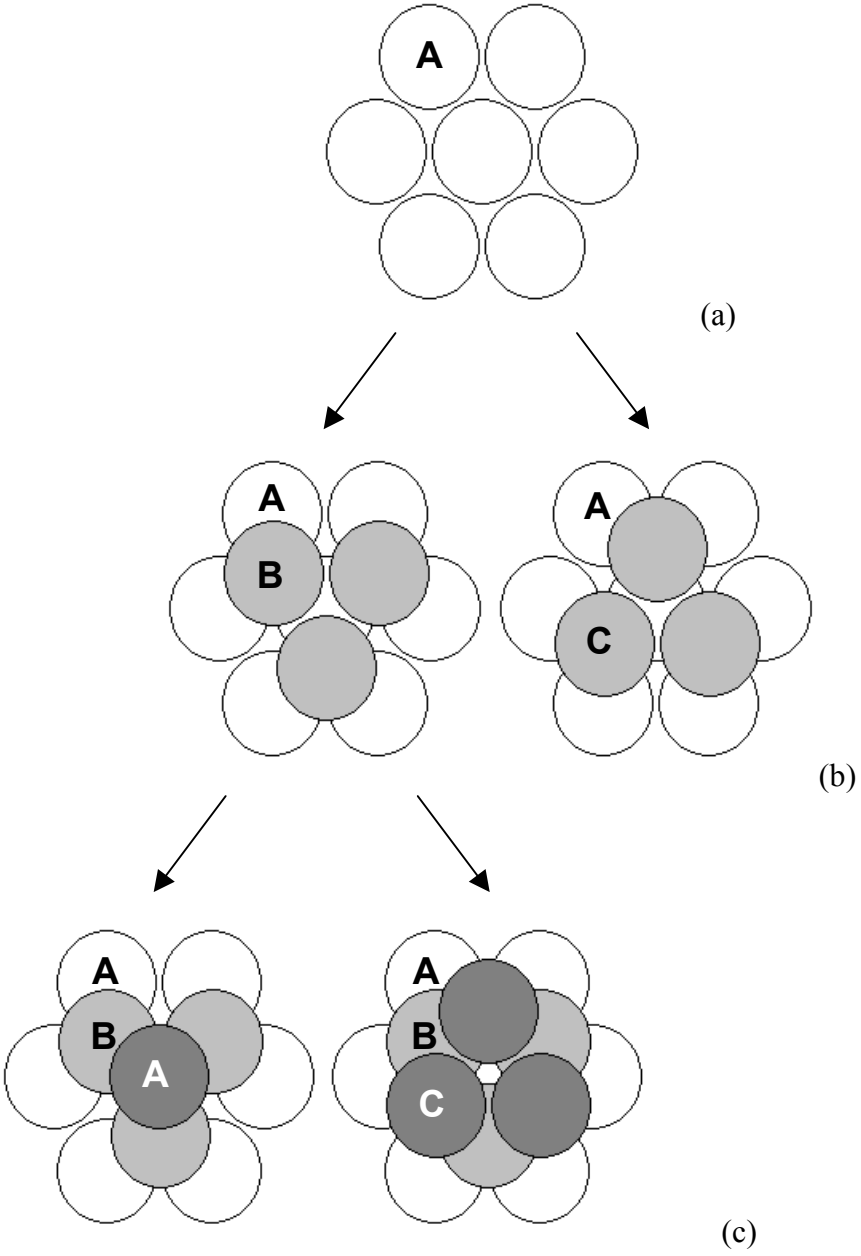

Figure I.1 : Formation of the FCC and BCC structures by the superposition of close-packed planes : (a) one, (b) two and (c) three planes.

I.1.2 Influence of temperature, chemical composition and applied stress

At a given pressure and without externally applied stress, the temperature and the chemical composition determine the equilibrium. For example, at 800°C, pure iron exhibits a fully austenitic structure but the ferritic phase becomes more stable s the temperature decreases. Additions of some elements, such as Cr, Si, Al, Mo, Nb, Ti,… favour the formation of ferrite (alpha-stabilizers) while others, such as Ni, C, Mn, N, Cu,… stabilize the austenite (gamma-stabilizers) [Laco90]. In stainless steels, the stabilizing effect of alloying elements is compared to the stabilizing effect of chromium or nickel, respectively. This provides the relative coefficients used in the calculation of the "equivalent chromium" and the "equivalent nickel", formulas which quantify the alpha or gamma stabilizing effect of a given composition. Several empirical formulas exist and some of them are presented in Table I.1 [Caba04].

Author	Equivalent Ni	Equivalent Cr
Schaeffler	%Ni + 30 · %C + 0.5 · %Mn	%Cr + 1.5 · %Si + %Mo + 0.5 · %Nb
De Long	%Ni + 30 · (%C + %N) + 0.5 · %Mn	%Cr + 1.5 · %Si + 1.4%Mo + %Nb + 2 · %Ti
Schneider	%Ni + 30 · %C + 25 · %N + 0.5 · %Mn + %Co + 0.3 · %Cu	%Cr + 2 · %Si + 1.5 · %Mo + 1.75 · %Nb + 1.5 · %Ti + 5.5 · %Al + 5 · %V + 0.5 · %W

Table I.1 : Empirical formulas for calculation of equivalent Ni and equivalent Cr [Caba04].

Four different types of stainless steels can be distinguished, depending on the number and type of phases present in the microstructure : martensitic, ferritic, austeno-ferritic (or “duplex”) and fully austenitic stainless steels. The resulting microstructure will be determined by two factors : the chemical composition and the thermo-mechanical process. The austenitic grades present improved mechanical properties so that they can be good candidates for structural applications. However, expensive alloying elements like nickel can hinder their extensive use. In order to keep high mechanical performances at a lower cost, the replacement of some elements has been investigated. This leads to the development of other highly alloyed steel grades. For example, Fe-Mn-Al alloys combine low price and acceptable corrosion resistance, so that it can be a good candidate

for the replacement of conventional Ni-Cr stainless steels for applications where the corrosion resistance is not critical [Chen93]. Indeed, a regenerative surface coating of alumina is created on the surface, which plays the same role but with a lower resistance to corrosion than the chromium oxide layer in stainless steels [Pete97]. Additions of chromium or chromium and nickel to these alloys have been reported to improve the corrosion resistance, especially for non-magnetic and cryogenic alloys [Zhan02]. However, the yield strength of Fe-Mn-Al grades are much lower than commercial Ni-Cr steels [Char81], and mechanically-induced phase transformations are reduced due to the aluminium additions. Therefore, other alloying elements may be added to increase the mechanical properties and retrieve the transformation phenomena such as silicon [Gräs98], carbon [Kim89] or niobium [Kim85]. However, it must be noted that the addition of interstitial elements such as carbon or nitrogen also induce a higher fragility in the Fe-Mn-Al alloys [Char82].

At low temperatures, *i.e.* when the thermal activity of diffusion ceases to be sufficient, the transformation of the austenite occurs by martensitic transformations. A martensitic transformation is a displacive and diffusionless transformation consisting in a cooperative shear movement of atoms on distances lower than the interatomic distance of the crystal lattice. Therefore, the mother and daughter phases present the same chemical composition. The atoms move in an organised manner relative to their neighbours. It induces a change of the crystallographic structure from the austenite (FCC) to the ε-martensite (HCP) or to the α'-martensite (BCC). Moreover, another

martensitic transformation is possible, from the ε-martensite to the α'-martensite [Bree71]. The structure of the martensite formed also depends on the chemical composition. For example, a Mn content over 16wt.% induces the formation of ε-martensite instead of α'-martensite in Fe-Mn alloys, as shown by Figure I.2 [Verc04].

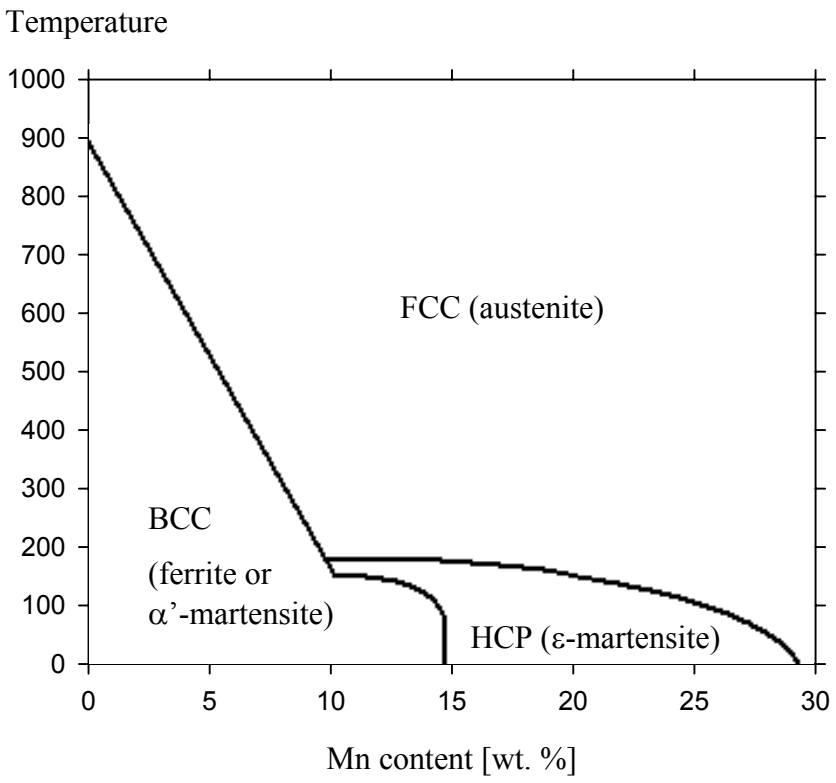

Figure I.2 : Metastable Fe-Mn binary phase diagram [Verc04]. The transition lines represent the start temperature for the phase transformation (martensitic or not).

As an example, Figure I.3 schematically presents the evolution of the free energies of austenite and α'-martensite as a function of temperature. At higher temperatures, the austenite presents the lowest free energy. The T_0 temperature corresponds to the temperature where the free energy of both phases are identical. The transformation of γ into α' is thus possible for temperatures lower than T_0. However, the existence of non-chemical energy barriers, such as interfacial energy and elastic energy, require the application of a driving force larger than a minimum free energy (ΔG_{crit} on Figure I.3) to initiate the martensitic transformation. ΔG_{crit} corresponds to $\Delta G_{ch,Ms}$, *i.e.* the difference of chemical free energy between austenite and martensite at the M_s temperature. For temperatures below M_s, the martensitic transformation takes place spontaneously, bringing about athermal martensite. For temperatures between T_0 and M_s, the austenite will remain in a metastable state. However, the complementary free energy can be provided by a mechanical contribution. Indeed, at a temperature T_1, a mechanical driving force U resulting from the application of an external stress may compensate the lack of chemical driving force and induce the martensitic transformation [Jacq98]. This required mechanical energy can be defined as $U = (\Delta G_{crit} - \Delta G_{ch,T})$. The maximum of mechanical energy (U^{max}) that can be provided to the material is limited by its mechanical behaviour. The temperature M_d can be defined as the temperature at which $U = U^{max}$ (as shown on Figure I.3). Above M_d, the transformation can not be induced mechanically [Jacqu98, Han04].

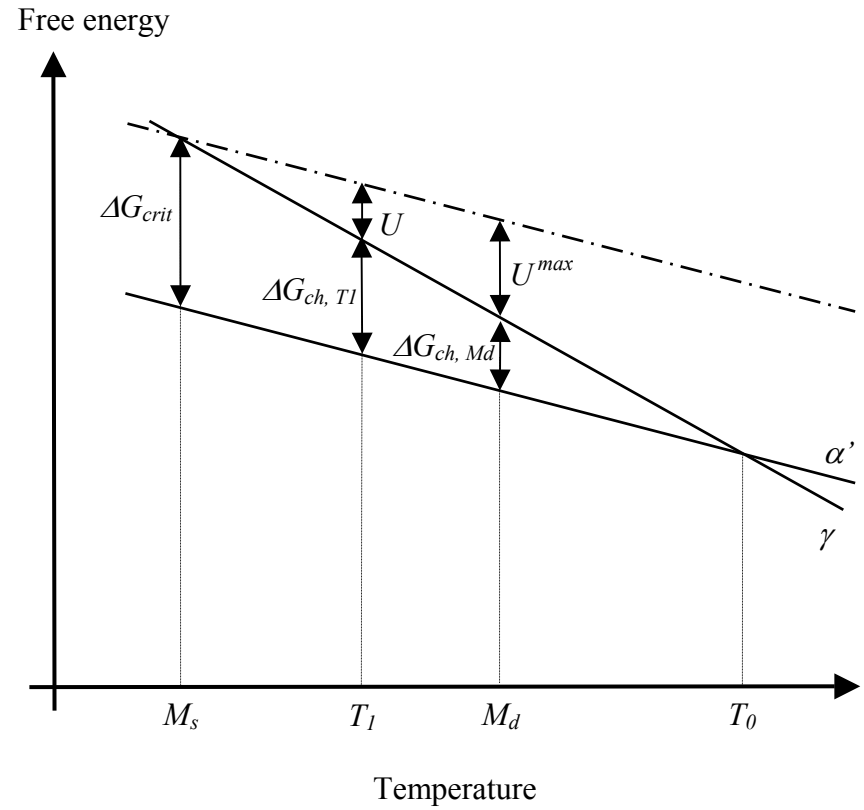

Figure I.3 : Schematic illustration of the chemical free energies of undeformed austenite (γ) and α'-martensite as a function of temperature (after [Jacq98]).

Finally, magnetic effects may also influence the phase stability. Indeed, the ε phase is anti-ferromagnetic, the ferrite α is ferromagnetic and the austenite is either paramagnetic or anti-ferromagnetic. A transition between paramagnetic and anti-ferromagnetic states takes place for the austenite at the Néel temperature (T_N). Below T_N, the thermal expansion coefficient of the austenite is lowered and its entropy is reduced by magnetic ordering [Chen99]. These phenomena

decrease the free energy of austenite and stabilize the austenite against phase transformation. This can be observed by the evolution of the transition temperatures according to the Mn content in Fe-Mn alloys, such as shown on Figure I.4 (from [Cote04]). The alloys that transform from or to the paramagnetic austenite show M_s and A_s temperatures that decrease almost linearly when the Mn content increases. However, alloys that transform from a ferromagnetic austenite (under T_N) show M_s temperatures that rapidly deviate from the linear behaviour, due to the influence of the magnetic stabilizing effect. Moreover, depending on the alloy composition, the M_s temperature can be lower than the Néel temperature so that the thermal formation of martensite may be completely suppressed and the stress-induced martensite formation reduced or prevented [Chen99, Wu00].

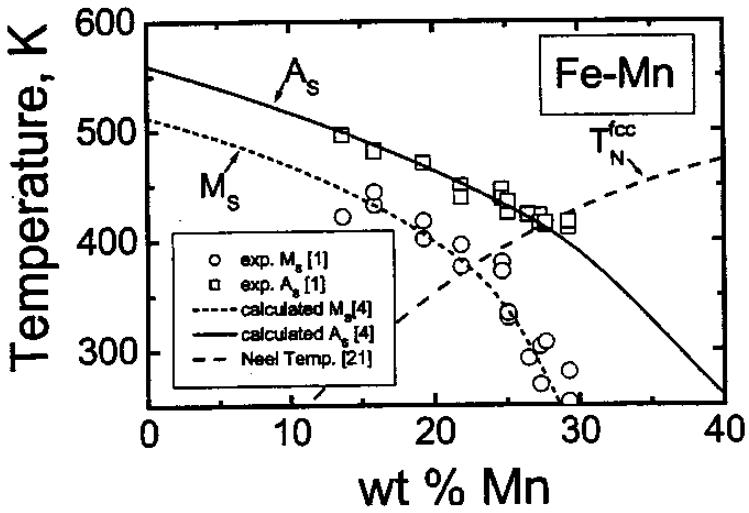

Figure I.4 : Evolution of A_s, M_s and T_N with the Mn content and the temperature (from [Cote04]).

Olson and Cohen have suggested a way to differentiate the mechanisms of formation of the mechanically-induced martensite [Olso72]. Figure I.5 shows the evolution of the critical stress required to initiate martensitic transformation between M_s and M_d. For temperatures comprised between M_s and M_s^σ, the applied stress required to initiate the transformation is smaller than the austenite yield strength. In this temperature range, the required level of stress increases linearly with the temperature [Pate53]. The transformation is said to be "stress-assisted" and the nucleation of the martensite is supposed to take place on the same nucleation sites responsible for the athermal martensite [Olso72, Naru82]. M_s^σ is defined as the temperature at which the critical stress required to initiate the transformation reaches the austenite yield strength. From this temperature, the austenite starts to deform plastically before the occurrence of the transformation. New nucleation sites for martensitic transformation are created by the deformation of the austenite. Thanks to this multiplication of nucleation sites, the critical level of stress is smaller than the expected level obtained by extrapolating the evolution of critical stress observed between M_s and M_s^σ. The transformation is then said to be "strain-induced". In metastable fully austenitic steels, M_s^σ can be easily determined from the reversal in the temperature dependence of the macroscopic (0.2%) flow stress [Rich71, Haid89].

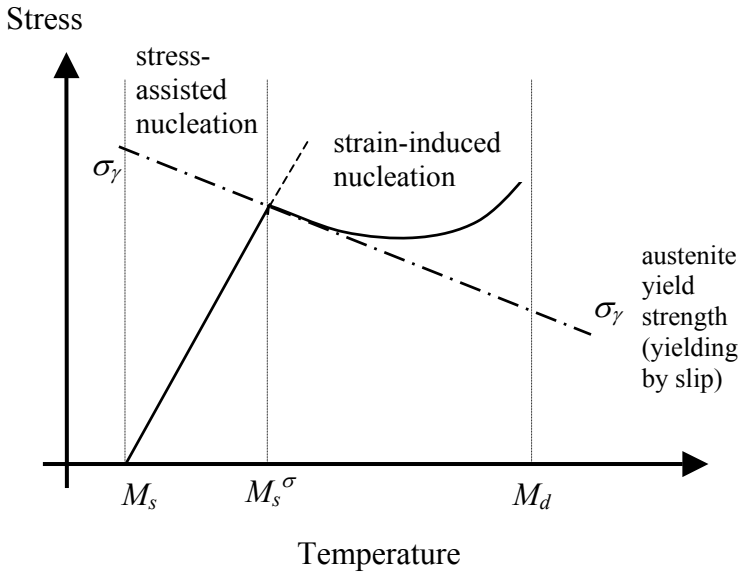

Figure I.5 : Schematic illustration of the different regimes of mechanically-induced martensite transformation as a function of temperature (after [Olson72]).

In order to predict the behaviour of some steel grades, some empirical formulas have been proposed to predict M_s and M_d temperatures from their chemical compositions. These formulas are valid only within a restricted range of composition. Furthermore, as M_d is difficult to determine precisely, it is sometimes replaced by $M_{d(30)}$, *i.e.* the temperature at which 50% of the austenite would have been transformed into martensite after a true strain of 30%. For example, the equations giving M_s and $M_{d(30)}$ for transformation of austenite into α'-martensite in stainless steels [Laco90] are written as :

$$M_s \text{ (in °C)} = 1302 - 42\ (\text{wt.\% Cr}) - 61\ (\text{wt.\% Ni}) - 33\ (\text{wt.\% Mn}) - 28\ (\text{wt.\% Si}) - 1667\ (\text{wt.\% C} + \text{wt.\% N}) \quad \text{(I.1)}$$

$$M_{d(30)} \text{ (in °C)} = 413 - 462\ (\text{wt.\%C} + \text{wt.\%N}) - 0.2\ (\text{wt.\%Si}) - 8.1\ (\text{wt.\%Mn}) - 13.7\ (\text{wt.\%Cr}) - 0.5\ (\text{wt.\%Ni}) - 18.5\ (\text{wt.\%Mo}) \quad \text{(I.2)}$$

which are valid for the compositions : 10 to 18 wt.%Cr, 6 to 12 wt.%Ni, 0.6 to 5 wt.%Mn, 0.3 to 2.69 wt.%Si, 0.004 to 0.12 wt.%C and 0.01 to 0.06 wt.%N.

I.2 Stacking fault energy

Different mechanisms are related to the irreversible deformation of a FCC lattice : dislocation glide, dissociation of dislocations into partial dislocations, mechanical twinning and mechanically-induced phase transformations. The parameter determining which phenomenon is activated during straining is the stacking fault energy.

I.2.1 Description of a stacking fault

A *stacking fault* is a lattice defect, defined by a mistake in the succession of planes. There are two different types of stacking faults in FCC metals : *intrinsic* and *extrinsic*. Figure I.6 shows an intuitive representation of intrinsic (Figure I.6 (a)) and extrinsic (Figure I.6 (b)) stacking faults. An intrinsic stacking fault is similar to the suppression

of a plane in the stacking. On the contrary, an extrinsic stacking fault is similar to the addition of a supplementary plane in the stacking.

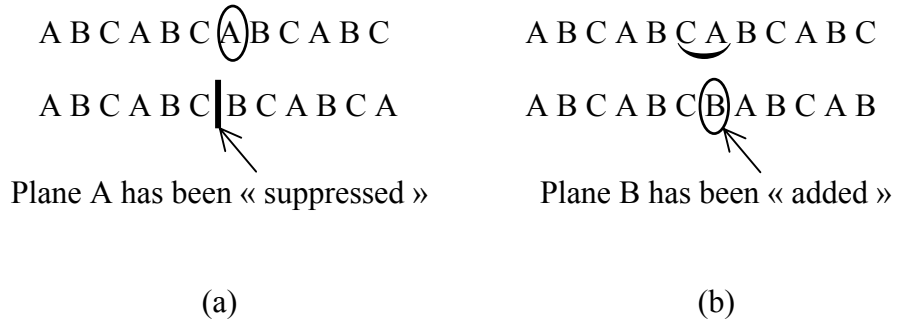

Figure I.6 : Intrinsic (a) and extrinsic (b) stacking faults in FCC metals.

The excess of energy brought about by the stacking fault is called the *stacking fault energy* (SFE). As two different stacking faults may be found (intrinsic and extrinsic), two different SFE could be defined [Blan90]. However, as the intrinsic SFE is generally lower than the extrinsic one, different materials are compared based on their intrinsic SFE [Remy77]. Several parameters influence the SFE, like the chemical composition and the temperature, but also the grain size.

I.2.2 Influence of various parameters on the stacking fault energy

I.2.2.1 Chemical composition

Austenite-stabilizing elements also have a large influence on the SFE. For example, nickel and carbon increase the SFE, while chromium and nitrogen decrease it [Laco90]. In the Fe-Mn-Si-Al steel

grades studied in this thesis, three alloying elements are present : Al, Si and Mn. Al increases the SFE [Cha81, Oh95, Chen93]. On the other hand, Si decreases the SFE [Furu89, Gräs98, From03]. The effect of Mn additions is more controversial. Indeed, several studies [Tomo86, Tomo91, Lee00, Cote04] showed that increasing the manganese content in Fe-Mn alloys first tends to decrease the SFE down to a minimum before increasing it again. However, the reported critical Mn content at which the SFE is minimised varies from 3 to 21 at.% Mn, while the reported minimum value of SFE varies from 11 to 22 mJ/m². Figure I.7 presents the influence of the Mn content on the SFE according to Schumann [Cote04]. The minimum SFE (11mJ/m²) is reached for a Mn content of about 14 at.% (or 13.8wt.%).

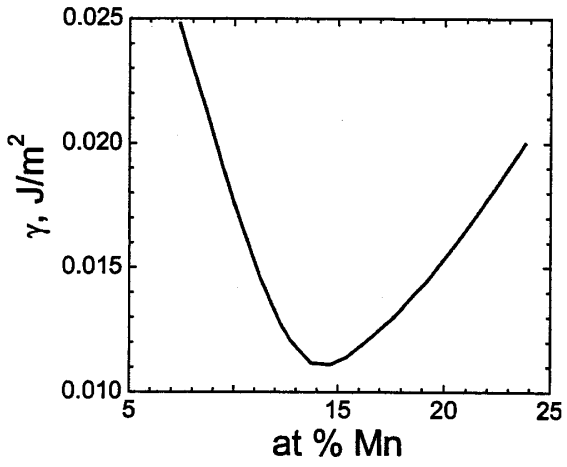

Figure I.7 : Evolution of the SFE with the Mn content of Fe-Mn alloys. (from [Cotes04])

Finally, the proportion of carbon has a large influence on the stacking fault energy in Fe-Mn alloys [Char82] and for a constant manganese content, additions of carbon increase the stacking fault energy.

In austenitic stainless steels, Schramm and Reed [Schr75] compiled the values of measured SFE in different alloys into a linear relationship based on the chemical compositions of Fe-Ni-Cr-Mn grades :

$$\text{SFE (in mJ/m}^2\text{)} = -53 + 0.7\,(\%\,\text{Cr}) + 6.2\,(\%\,\text{Ni}) + 3.2\,(\%\,\text{Mn}) + 9.3\,(\%\,\text{Mo}) \qquad \text{(I.3)}$$

However, according to Rhodes and Thompson [Rhod77], this method would not be reliable due to the complex and generally non-linear relationship between the alloying element content and the SFE in austenitic stainless steels, except for some Fe-Ni-Cr ternary alloys. As an improvement of the Schramm and Reed equation, they suggest to use iso-SFE surfaces in the Fe-Ni-Cr ternary diagram. However, based on the work of Schramm and Reed and on their own data, they propose a corrected version of eq. I.3, which would be applicable for alloys containing 18% or more Cr and significant Mn and Si contents :

$$\text{SFE (in mJ/m}^2\text{)} = 1.2 + 0.6\,(\%\,\text{Cr}) + 1.4\,(\%\,\text{Ni}) + 17.7\,(\%\,\text{Mn}) - 44.7\,(\%\,\text{Si}) \qquad \text{(I.4)}$$

I.2.2.2 Temperature

Figure I.8 presents the evolution of the SFE with temperature in high-manganese steels reported by Tomota [Tomo91]. It can be observed that the SFE increases with temperature, with a steep rise occurring just above room temperature. This steep rise is particularly marked for steels with lower Mn contents.

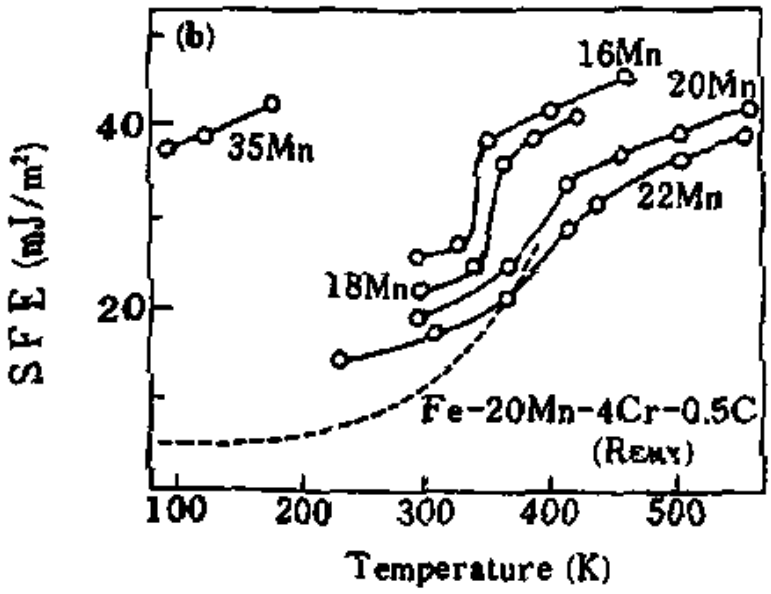

Figure I.8 : Evolution of the SFE with the temperature for different Fe-Mn alloys (from [Tomo91]).

Although it is well known that SFE increases with temperature, there is a lack of accurate data concerning this evolution for stainless steels. Dai *et al.* [Dai03] suggested that a first approximation could be given by :

$$SFE = SFE_1 + 0.07\,(T - T_1) \qquad \text{(I.5)}$$

with SFE_1 being the SFE at room temperature T_1.

I.2.2.4 Austenite grain size

Grain size has also been reported as an influencing parameter on the SFE. According to Jiang *et al.* [Jian98], the SFE is independent of the grain size in Fe-Mn-Si alloys. However, most of the studies indicate the opposite behaviour [Noha76, Cote95, Naka96a, Naka96b, MnLR96, Jun98, Lee00]. The evolution of the SFE with the austenite grain size is shown by Figure I.9 (a) in Fe-18%Mn alloy [Jun98] and by Figure I.9 (b) in Fe-17.8%Mn-0.47%C alloy [Lee00]. It can be seen that the SFE is almost constant for grain sizes larger than 40µm. However, it steeply increases below 40µm. A first explanation, given by Volosevich *et al.* [Volo76], would be the influence of internal stresses, which may vary in amplitude according to the grain size and prevent the dissociation of dislocations. In addition to this explanation, Lee *et al.* [Lee00] mentioned that the grain size could represent a geometric obstacle against the dissociation of dislocations if the grain size is smaller than the equilibrium width of stacking faults. In this case, the dislocations would not be able to dissociate completely, leading to a rise of the SFE.

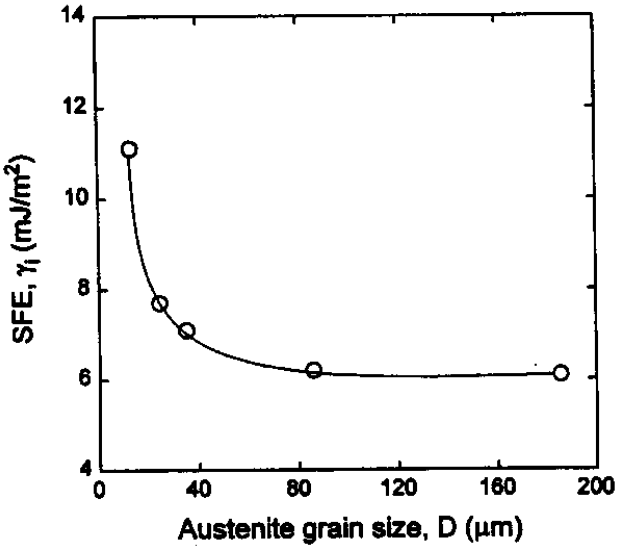

(a)

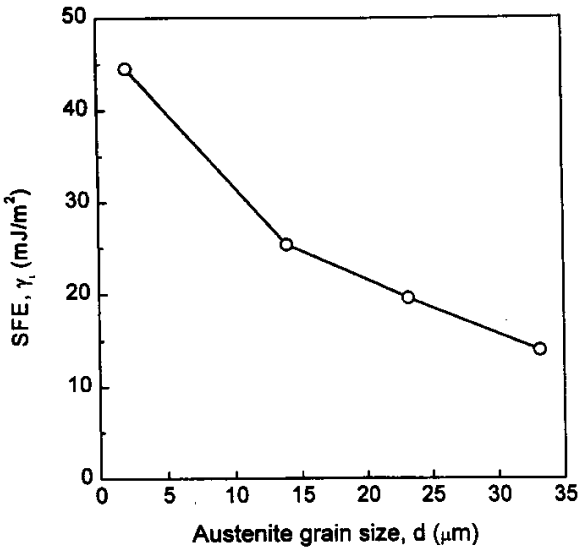

(b)

Figure I.9 : Evolution of the SFE with the austenite grain size in (a) Fe-18%Mn (from [Jun98]) and (b) Fe-17.8%Mn-0.47%C (from [Lee00]) alloys.

I.2.3 Effect of the stacking fault energy on the deformation modes

I.2.3.1 Dislocations and partial dislocations

The most common deformation mode implies the movement of dislocations. As it is shown on Figure I.10, a *dislocation* consists in a supplementary half-plane distorting the regular stacking.

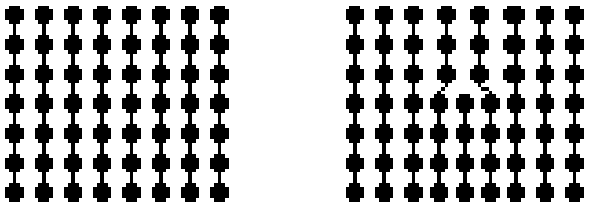

(a) (b)

Figure I.10 : Illustration of a dislocation in a crystal lattice : (a) unfaulted lattice ; (b) lattice with a dislocation.

The movement of a dislocation requires that one atom moves from its position to the next similar position. The possible positions are determined by the lattice symmetry, defining a restricted amount of planes in which the dislocation core can glide. As shown on Figure I.11, on a very local basis, energy barriers exist against the movement of the dislocation core, corresponding to the presence of the other lattice atoms. Dislocations can then tend to separate into two partial dislocations (or Shockley dislocations) to reduce the energy required for their movements. The result of both movements correspond to a glide of the dislocation by one Burgers vector. When the leading

partial dislocation goes through the lattice, it moves an atom into an intermediary position (the broken circle on Figure I.11), corresponding to another stacking plane : a stacking fault is then created after the passage of the leading partial dislocation. After the trailing partial dislocation, the atom is back to its original stacking plane and the stacking fault is annihilated.

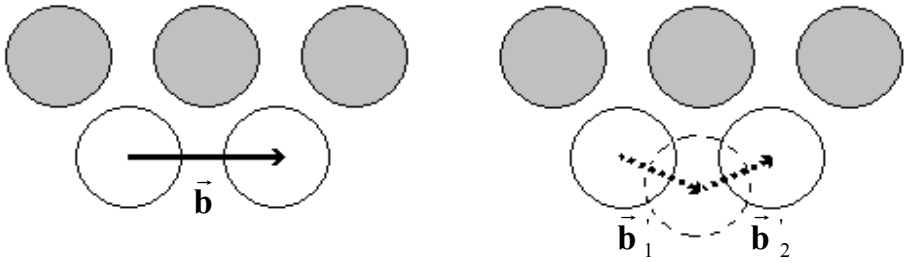

Figure I.11 : Dissociation of a dislocation (Burgers vector $\vec{b}$) into 2 partials ($\vec{b}'_1$ and $\vec{b}'_2$).

The width of the stacking fault comprised between the two Shockley partial dislocations results from an equilibrium between the minimization of the lattice disorder caused by the stacking fault and the repulsive forces between both partial dislocations. If the SFE is very high, the dislocations tend to remain unparted. On the contrary, if the SFE is low, the dislocations part easily. However, the movement of the partial dislocations is limited to the only gliding plane containing both of them, which prevents dislocation climb or change of gliding plane. Therefore, partial dislocations tend to quickly build up stable substructures within the grains and further straining then triggers other deformation mechanisms.

I.2.3.2 Mechanical twins

Twins are characterised by a "mirror plane" separating a crystal in two symmetrical parts. Figure I.12 shows a twin representation where the mirror plane ***B*** is highlighted.

A B C A B C A B C A B C A B C A ***B*** A C B A C B A C B A C B

mirror plane

Figure I.12 : Twin in FCC metals.

Annealing twins are very common in FCC metals such as austenitic steels and copper. However, twins can also appear during plastic deformation, in materials presenting low SFE. Indeed, the mechanical twins may be formed by direct shearing of the austenite or by piling up of several intrinsic stacking faults [Blan90]. As the SFE is low, the density of stacking faults may be very high. Figure I.13 shows how intrinsic stacking faults (SF) packing on every (1 1 1) plane in austenite (FCC) brings about a mechanical twin.

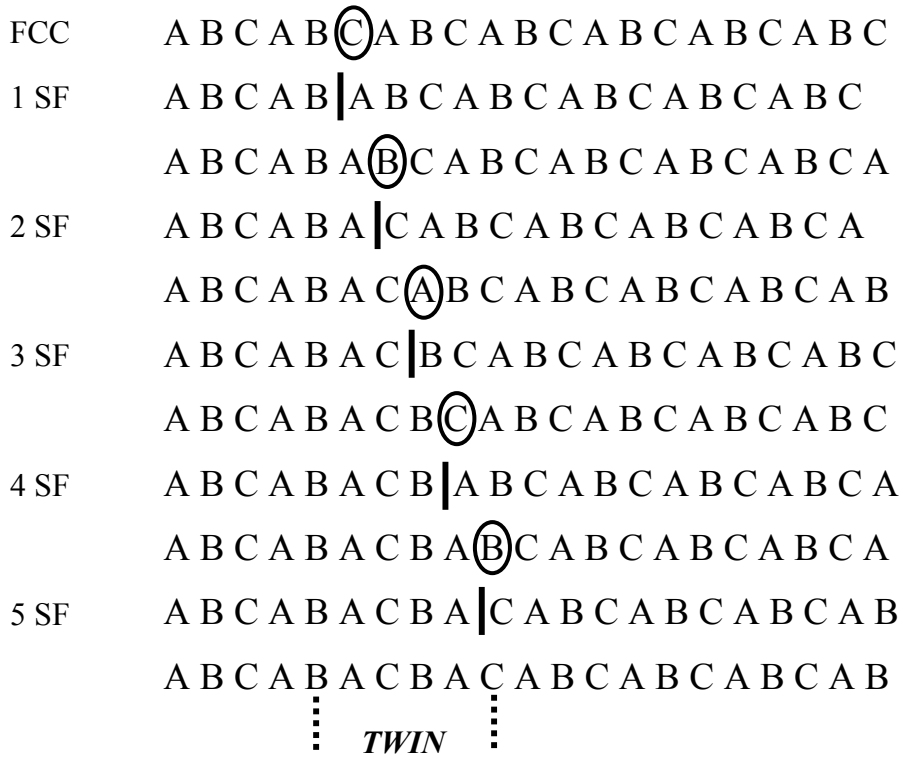

Figure I.13 : Schematic illustration of the formation of a mechanical twin by piling up intrinsic stacking faults.

I.2.3.3 Mechanically-induced martensitic transformation

Due to their role in this work, the mechanically-induced phase transformations will be detailed in section I.3. However, it must be anticipated that they also require the piling up of stacking faults. Therefore, martensitic transformations are also favoured by a low SFE.

I.2.3.4 Relationship between stacking fault energy and deformation mode

Each of the deformation modes requires a critical level of stress that must be reached locally to induce this mode. This critical level is different for the formation of dislocations, twins, ε- or α'-martensite. The active deformation mode is the one with the lowest critical stress in the local conditions, which explains why different modes may be active simultaneously throughout a strained specimen. As shown on Figure I.14, the active irreversible deformation mode goes successively from perfect and partial dislocations glide to mechanical twinning and finally mechanically-induced martensitic transformations with a decreasing value of SFE. It is usually admitted that the transformation into α'-martensite takes place for lower SFE than for ε-martensite [Gräs98, Gräs00, Verc04, Caba04]. However, the interactions between SFE and phase stability are not sufficiently taken into account. Indeed, it is possible to have the formation of α'-martensite even when the SFE is high enough to prevent the formation of ε-martensite [Choi97]. The evaluation of the sole influence of the SFE on the formation of ε- and α'-martensite has not been found in the literature.

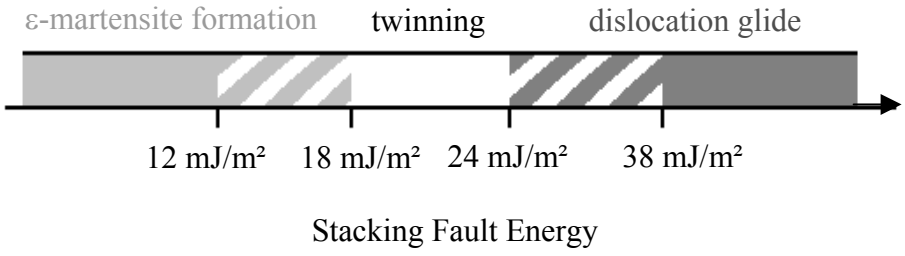

Figure I.14 : Active modes of plastic deformation as a function of the stacking fault energy (after [Caba04]).

I.3 Mechanically-induced martensitic transformation

In the case of high-manganese steels and austenitic stainless steels, two mechanisms have been reported for the mechanically-induced martensitic transformation : $\gamma \rightarrow \alpha$' or $\gamma \rightarrow \varepsilon (\rightarrow \alpha')$ [Vena62, Bree71, Tomo86, Cote95, Lee00, Jee01, Cote04]. This section will present successively the crystallographic mechanisms of transformations, the resulting orientation relationships between the mother and daughter phases and finally the influence of these transformations on the mechanical properties.

I.3.1 Crystallographic mechanisms

I.3.1.1 Transformation into ε-martensite

The formation of ε-martensite (HCP) can be explained by the interactions between stacking faults within a FCC lattice. Olson and

Cohen [Olso72] explained the formation of ε-martensite by the piling up of intrinsic stacking faults every second plane. This model did not elucidate the exact mechanisms of $\gamma \rightarrow \varepsilon$ transformation, but provided a plausible explanation of the transformation. Mahajan *et al.* [Maha77] suggested that two dislocations of different but co-planar Burgers vectors could dissociate and interact to form a 6 layers HCP region in austenite. This nucleus would then react with other similar nuclei, they would grow into each other and form a macroscopic crystal of ε-martensite. Brooks *et al.* [Broo79b] observed in situ the nucleation and growth of ε-martensite in stainless steels. They concluded that the ε-martensite may nucleate from a single stacking fault in the austenite. Figure I.15 shows how a stacking of extrinsic stacking faults (SF) every plane in the austenite may create a short sequence of hexagonal closed-packed (HCP) stacking in the FCC lattice, thereby explaining the formation of the ε phase. Therefore, the transformation of austenite into ε-martensite is favoured by a low SFE. It can be noticed that the stacking of extrinsic stacking faults every plane is equivalent from a crystallographic point of view to a stacking of intrinsic stacking faults every other plane.

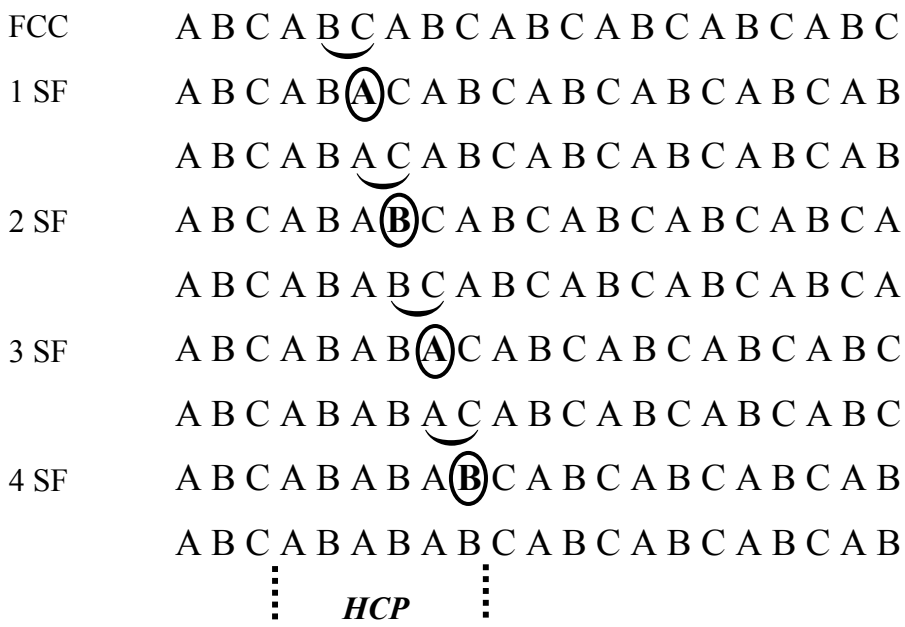

Figure I.15 : Schematic illustration of the stacking of extrinsic stacking faults that brings about a local hexagonal close-packed (HCP) lattice.

I.3.1.2 Formation of α'-martensite

Two mechanisms of transformation have been observed in stainless steels : direct transformation from austenite to α'-martensite and indirect transformation, with ε-martensite as an intermediary phase. The direct transformation of austenite into α'-martensite can not be explained by a simple piling up of stacking faults. However, Brooks *et al.* [Broo79b] concluded from *in situ* observation of the nucleation and growth of α'-martensite in stainless steels that it involves faulted regions in dislocation pile-ups. Indeed, they calculated that in a dislocation pile up, the partials may be forced

much closer together by the applied stress and the atomic structure close to the core of the slightly separated partials is then close to BCC stacking. Indeed, after half the shear imposed by a partial dislocation, the atoms of a FCC lattice appear in a pseudo BCC stacking as it is shown in Figure I.16 [Broo79a]. The volume of effective BCC structure then increases as more dislocations join the pile-up until the formed nucleus reaches a critical size and rapid growth takes place.

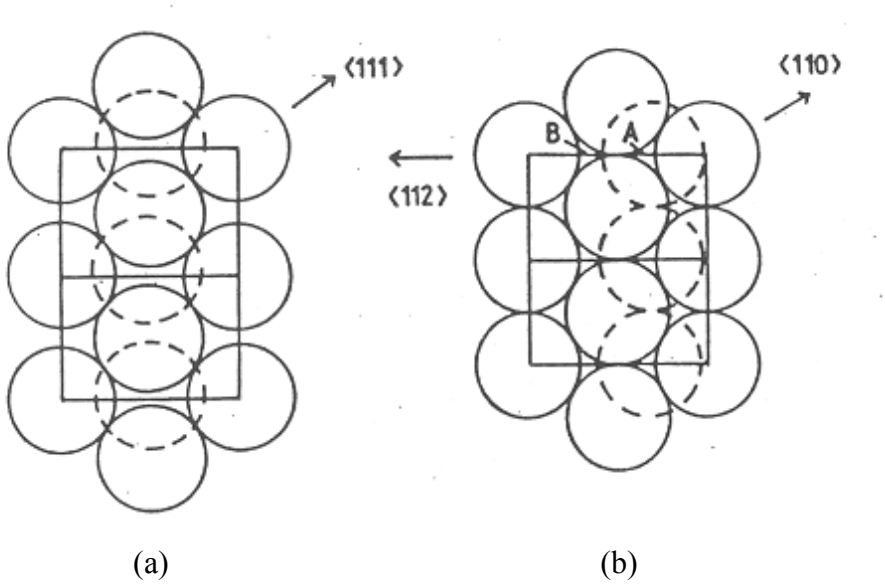

Figure I.16 : BCC (1 1 0) (a) and FCC (1 1 1) (b) planes with two crystallographic units (squares) shown in each lattice. The shear brought about by a partial dislocation along the <1 1 2> direction moves the atoms from a "A" to a "B" position. After half of this shear, the atoms present a pseudo-BCC stacking (from [Broo79a].

Lecroisey and Pineau [Lecr72] showed that the laths of α'-martensite formed by plastic deformation are frequently located at the intersection of two deformation bands (platelets of ε phase, twins, shear bands or slip planes), where a nucleus of α'-martensite appears. TEM studies have indicated that microshear bands intersection within a grain are the preferred sites for the nucleation process during the deformation of 304 stainless steel [Onyu04]. Choi and Jin [Choi97] observed that intersections of mechanical twins can also bring about the formation of α'-martensite during cold drawing of 304 stainless steel. Numerous studies [Bree71, Olso72, Spen04] have shown that the intersections of bands of ε phase result in a local BCC structure, providing a nucleus for the formation of α' martensite. A shear of the ε phase may also be at the origin of the nucleation of α' martensite [Lee01a, Lee01b]. After nucleation, the α'-martensite grows either within the ε bands or by direct transformation of the austenite. According to Varma *et al.* [Varm94], the growth of the nuclei is also different from the conventional growth of precipitates and takes place by a process of coalescence of the nearby nuclei.

The transformation of austenite into α'-martensite is accompanied by a dilatation and a shear deformation [Pate53, Bowl54, Mack54]. Figure I.17 presents the Bain and Davenport mechanism explaining the transformation from a geometrical point of view : it corresponds to a rotation of the lattice, accompanied by a contraction of about 20% along the Z' axis and an expansion of about 12% along both X' and Y'.

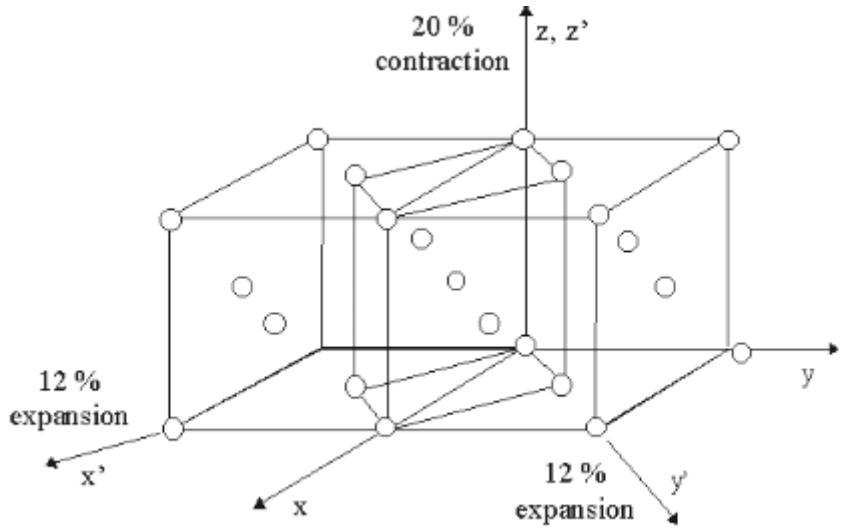

Figure I.17 : Bain and Daventport mechanism for γ to α' martensitic transformation (from [Laco90])

I.3.1.3 Orientation relationships

The transformation of the austenite can be described by the invariant plane, which is common to both the mother and the daughter phases (for example : the base plane in Figure I.17), and by the rotation of the crystal coordinate system. However, due to crystal symmetry properties, several planes and directions are equivalent. Therefore, one austenite orientation can bring about several equivalent martensite orientations, named *variants*. Different works have tried to establish rules describing the orientation relationships between the austenite and the daughter martensite, based on the crystallographic possibilities.

As far as direct transformations of austenite into α'-martensite are concerned, three main orientation relationships have been proposed [Gode03]. According to Bain, the FCC $\{001\}_\gamma$ planes are parallel to the BCC $\{001\}_\alpha$ planes, while the FCC $<001>_\gamma$ directions are parallel to the BCC $<110>_\alpha$ directions. These rules foresee the formation of three martensite variants issued from one austenite grain. Kurdjumov and Sachs (KS relationships) as well as Nishiyama and Wasserman (NW relationships) tried to refine the Bain predictions. The main difference with the Bain rules is that the invariant plane is now chosen to be a close-packed plane in both γ and α phases. According to the KS rules, FCC $\{111\}_\gamma$ and BCC $\{011\}_\alpha$, as well as FCC $<011>_\gamma$ and BCC $<111>_\alpha$ are parallel. Finally, according to the NW set of rules, it is FCC $\{111\}_\gamma$ and BCC $\{011\}_\alpha$, as well as FCC $<211>_\gamma$ and BCC $<011>_\alpha$ that are parallel. For each orientation of an austenite grain, the KS relationships predict the formation of 24 equivalent BCC variants, against 12 for the NW rules. A schematic representation of the orientation relationships between the austenite and the ferrite (or α'-martensite) lattices for all three models is given in Figure I.18. Other sets of rules have been presented, with crystallographically close orientations, but the most recent experiments [He06] demonstrate that the KS and NW relationships are most successful to describe the correlation between γ and α phases.

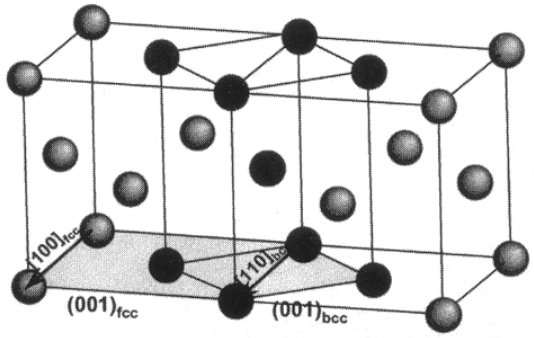

Bain orientation relations: $\{001\}_\gamma // \{001\}_\alpha$ and $<001>_\gamma // <110>_\alpha$

(*a*)

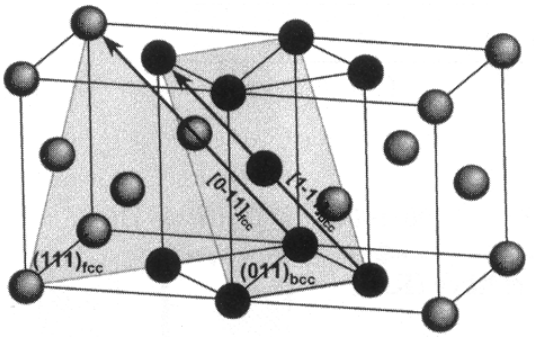

Kurdjumov-Sachs orientation relations: $\{111\}_\gamma // \{011\}_\alpha$ and $<011>_\gamma // <111>_\alpha$

(*b*)

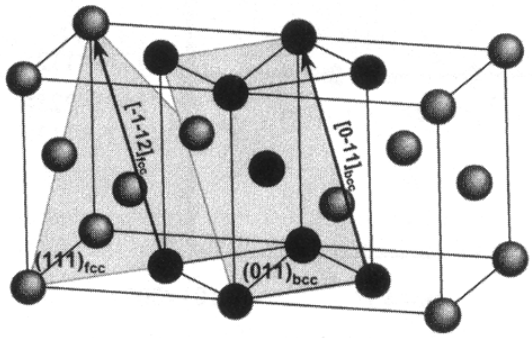

Figure I.18 : Schematic representation of orientation relationships between γ (FCC) and α (BCC) lattice : (a) Bain relationships ; (b) KS relationships and (c) NW relationships. The differences in lattice parameters are not shown for clarity reasons. (from [Gode03])

When the daughter martensite presents a HCP structure (ε-martensite), the same kind of orientation relationships exist between the compact plane and rotation direction of the γ and ε phases. In this case, the Burgers rules predict that FCC $\{111\}_\gamma$ and HCP $\{0001\}_\varepsilon$, as well as FCC $<1\text{-}10>_\gamma$ and HCP $<\text{-}12\text{-}10>_\varepsilon$ are parallel [Lecr72]. Some small differences in interatomic distances can be observed between the two structures but they are relatively easy to accommodate. The crystal symmetry shows that for one austenite orientation, 4 ε-martensite variants can be produced. In some cases, the ε-martensite transforms further into α'-martensite. Then, the orientation relationships show that BCC $\{011\}_\alpha$ and HCP $\{0001\}_\varepsilon$, as

well as BCC $<111>_{\alpha}$ and HCP $<-12-10>_{\varepsilon}$ are parallel, bringing about 6 different variants. It fits exactly with the 24 variants of the KS predictions.

I.3.2 TRIP effect and variant selection

The TRIP effect takes place when the progressive transformation of the austenite leads to plasticity. Indeed, the dilatation and shear provoked by the martensitic transformation may induce some plastic deformation in the material. In this way, mechanically-induced martensitic transformation acts as a plastic deformation mode in TRIP-assisted materials. Indeed, it has been shown that the volume change brought about by the transformation induces a dynamic softening in the material [Olso78, Naru82]. However, some recent studies [Bade02, Han04] showed that the importance of the contribution of the TRIP strain to the total elongation may be minimal (about 0.02 for a total strain of 0.45 [Han04]).

On the other hand, the mechanically-induced transformation of austenite into martensite is comparable to a "dynamic composite effect" due to the progressive appearance of the martensite during straining. Indeed, the yield strength of martensite is usually higher than of the austenite, allowing the martensite response to be completely elastic when subjected to levels of stress as observed in the material. Moreover, it creates new grain boundaries, which enhance the work-hardening. Finally, the surrounding austenite experiences a microscopic strain hardening due to the local plasticity provoked by the transformation volume variation, which is called the Greenwood-

Johnson effect [Gree65]. The appearance of martensite combined with the work-hardening of the surrounding matrix strongly increase the work-hardening of the material. The instability condition is thus fulfilled much later. The combination of all these effects increase the uniform deformation of TRIP-assisted steels as well as their strength [Bhan72, Tamu92].

Due to symmetry reasons in the lattice structures, several martensite orientations may be produced by the phase transformation. In reality, transformation texture measurements show that the variants are not equiprobable : some variants seem to be favoured during the transformation [Butr97, Gode03]. This phenomenon is called the *variant selection*. Due to the volume change it brings about in the crystal, the phase transformation is sensitive to both shear and normal components of the applied stress. These shape changes are not isotropic and the variant which are favoured exhibit the most favourable orientations with respect to the applied stress [Mage68]. This phenomenon is known as the Magee effect. A variant is said to be favourably oriented with respect to the applied stress when the orientation of the accompanying shear and volume change could be produced by a stress which is the closest to the applied stress. For example, Goodchild *et al.* [Good70] observed a strong variation in the transformation processes in stainless steels according to the orientation of the grains with respect to the applied stress. The transformation of austenite into ε-martensite is favoured when the applied tensile stress is parallel to $<110>_{\gamma}$ while the transformation is prevented if the applied tensile stress is parallel to $<100>_{\gamma}$. A

compressive stress applied in a direction parallel to $<100>_\gamma$ brings about ε-martensite.

I.4 Conclusion

In this Chapter, we have tried to give a first insight into the characteristics of stainless steels and highly alloyed steels exhibiting a TRIP-effect. The key of the excellent mechanical properties displayed by these grades relies on the presence of metastable austenite. The influence of the phase stability and of the stacking fault energy on the phase transformations and the consequences of these transformations on the mechanical properties of the material have been briefly described. The multiple interactions between chemical composition, testing temperature and grain size on the phase transformations represent both a real difficulty and a great source of opportunities in the use of these alloys. The following chapters will focus on these three parameters and try to show how the mechanical properties may be affected through a fine control of the microstructure.

References

[Bhan72] D. Bhandarkar, V. F. Zackay and E. R. Parker, *Metall. Trans.*, 1972, Vol. 3, p. 2619.

[Blan90] M. Blanc, *Mécanismes de déformation des aciers inoxydables austénitiques* in *Les aciers inoxydables*, 1990, edited by P. Lacombe, B. Baroux and G. Beranger for « Les editions de Physique », p. 613.

[Bowl54] J. S. Bowles and J. K. Mackenzie, *Acta Metal.*, 1954, Vol. 2, p. 224.

[Bree71] J. F. Breedis and L. Kaufman, *Met. Trans.*, Vol. 2, 1971, p. 2359.

[Butr97] M. P. Butrón-Guillén, C. S. Da Costa Viana and J. J. Jonas, *Metal. Mater. Trans.*, 1997, Vol. 28A, p. 1755.

[Broo79a] J. W. Brooks, M. H. Loretto and R. E. Smallman, *Acta Metal.*, 1979, Vol. 27, p. 1829.

[Broo79b] J. W. Brooks, M. H. Loretto and R. E. Smallman, *Acta Metal.*, 1979, Vol. 27, p. 1839.

[Caba04] N. Cabañas Poy, **Compositional effects on Structure-Property relationships in Mn-based austenitic ferrous alloys**, PhD Thesis, Ghent University, 2004.

[Char81] J. Charles and A. Berghezan, *Cryogenics*, 1981, p. 278.

[Char82] J. Charles, **Recherche de nouvelles nuances d'aciers austénitiques riches en manganèse et exempts de nickel pour des applications en cryogénie**, PhD Thesis, UCL, 1982.

[Chen93] F. C. Chen, C. P. Chou, P. Li and S. L. Chu, *Mater. Sci. Eng. A*, Vol. 160, 1993, p. 261.

[Chen99] S. Chen, C. Y. Chung, C. Yan and T. Y. Hsu (Xu Zuyao), *Mater. Sci. Eng. A*, Vol. 264, 1999, p. 262.

[Choi97] J. Y. Choi and W. Jin, *Scripta Mat.*, 1997, Vol. 36, No. 1, p. 99.

[Cote95] S. Cotes, M. Sade and A. Fernández Guillermet, *Metal. and Mater. Trans. A*, 1995, Vol. 26A, p. 1957.

[Cote04] S. Cotes, A. Fernández Guillermet and M. Sade, *Metal. and Mater. Trans. A*, 2004, Vol. 35A, p. 83.

[Dai03] Q. X. Dai, X. N. Cheng, X.M. Luo and Y. T. Zhao, *Materials Characterization*, Vol. 49, 2003, p. 367.

[From03] G. Frommeyer, U. Brüx and P. Neumann, *ISIJ International*, 2003, Vol. 43, p. 438.

[Furu89] T. Furukawa, *Materials Science and Technology*, 1989, Vol. 5, p. 465.

[Gode03] S. Godet, **Thermomechanical processing of TRIP-assisted multiphase steels**, PhD Thesis, UCL, 2003.

[Good70] D. Goodchild, W. T. Roberts and D. V. Wilson, *Acta Metal.*, 1970, Vol. 18, p. 1137.

[Gräs98] O. Grässel and G. Frommeyer, *Materials Science & Technology*, 1998, Vol. 14, p. 1213.

[Gräs00] O. Grässel, L. Krüger, G. Frommeyer and L. W. Meyer, *International Journal of Plasticity*, 2000, Vol. 16, p. 1391.

[Gree65] G.W. Greenwood and R. H. Johnson, *Proc. Roy. Soc. London*, *Ser. A*, 1965, Vol. 283, p. 403.

[Han04] H. N. Han, C. G. Lee, C. S. Oh, T. H. Lee and S. J. Kim, *Acta Mat.*, Vol. 52, 2004, p. 5203.

[Haid89] G. N. Haidemenopoulos, M. Grujicic, G. B. Olson and M. Cohen, *Acta Metal.*, 1989, Vol. 37, No. 6, p. 1677.

[He06] Y. He, S. Godet, P. J. Jacques and J. J. Jonas, *Acta Mat.*, 2006 , Vol. 54, No. 5, p.1323.

[Jacq98] P.J. Jacques, **On the physics and mechanics of phase transformations in TRIP-assisted multiphase steels**, PhD Thesis, UCL, 1998.

[Jee01] K. K. Jee, J. O. Song, W. Y. Jang, M. C. Shin and C. S. Choi, *Journal de Physique IV*, 2001, Vol. 11, p. 211.

[Jian98] B. Jiang, X. Qi, S. Yang, W. Zhou and T. Y. Hsu (Xu Zuyao), *Acta Mat.*, 1998, Vol. 46 No. 2, p. 501.

[Jun98] J. H. Jun and C. S. Choi, *Mater. Sci. Eng. A*, 1998, Vol. 257, p. 353.

[Kim85] Y. G. Kim, Y. S. Park and J. K. Han, *Metall. Trans.*, 1985, Vol. 16A, p. 1689.

[Kim89] Y. G. Kim, J. M. Han and J. S. Lee, *Mater. Sci. Eng. A*, 1989, Vol. 114, p. 51.

[Laco90] **Les aciers inoxydables**, 1990, edited by P. Lacombe, B. Baroux and G. Beranger for « Les editions de Physique ».

[Lecr72] F. Lecroisey and A. Pineau, *Metal. Trans.*, 1972, Vol. 3, p. 387.

[Lee00] Y. K. Lee and C. S. Choi, *Metal. and Mater. Trans. A*, 2000, Vol. 31A, p. 355.

[Lee01a] E. H. Lee, M. H. Yoo, T. S. Byun, J. D. Hunn, K Farrell and L. K. Mansur, *Acta Mat.*, 2001, Vol. 49, p. 3269.

[Lee01b] E. H. Lee, T. S. Byun, J. D. Hunn, M. H. Yoo, K Farrell and L. K. Mansur, *Acta Mat.*, 2001, Vol. 49, p. 3277.

[Mage68] C. L. Magee and H. W. Paxton, *Trans. Metall. Soc. AIME*, 1968, Vol. 242, p. 1741.

[Mack54] J. K. Mackenzie and J. S. Bowles, *Acta Metal.*, 1954, Vol. 2, p. 138.

[Maha77] S. Mahajan, M. L. Green and D. Brasen, *Met. Trans. A*, 1977, Vol. 8A, p. 283.

[MnLR96] **Manganese Literature Review**, No. 43, International Manganese Institute, 1996, p. 1.

[Noha76] K. Nohara, Y. Ono and N. Ohashi, *Symposium on « New aspects of martensitic transformations »*, 1976, p. 315.

[Naka96a] H. Nakatsu, T. Miyata and S. Takaki, *J. Japan Inst. Metals*, 1996, Vol. 60 No. 10, p. 928.

[Naka96b] H. Nakatsu, T. Miyata and S. Takaki, *J. Japan Inst. Metals*, 1996, Vol. 60 No. 10, p. 936.

[Naru82] T. Narutani, G. B. Olson and M. Cohen, *Journal de Physique*, 1982, Vol. 43 No. 12, p. 429.

[Olso72] G. B. Olson and M. Cohen, *J. Less-Comm. Met.*, 1972, Vol 28, p. 107.

[Olso78] G. B. Olson and M. Azrin, *Met. Trans. A*, 1978, Vol. 9A, p. 713.

[Oh95] B. W. Oh, S. J. Cho, Y. G. Kim, Y. P. Kim, W. S. Kim and S. H. Hong, *Mater. Sci. Eng. A*, 1995, Vol. 197, p. 147.

[Onyu04] M. Onyuna, H. Oettel, U. Martin and A. Weiss, *Advanced Engineering and Materials*, 2004, Vol. 6 No. 7, p. 529.

[Pate53] J. R. Patel and M. Cohen, *Acta Metall.*, 1953, Vol 1, p. 531.

[Pete97] M. A. Peters and H. W. King, *Canadian Metallurgical Quaterly*, 1997, Vol. 36 No. 1, p. 1.

[Remy77] L. Remy, *Acta Metal.*, 1977, Vol. 25, p. 173.

[Rich71] R. H. Richman and G. F. Bolling, *Met. Trans.*, 1971, Vol. 2, p. 2451.

[Rhod77] C. G. Rhodes and A. W. Thompson, *Met. Trans. A*, 1977, Vol. 8A, p. 1901.

[Schr75] R. E. Schramm and R. P. Reed, *Metallurgical Transactions A*, 1975, Vol. 6A, p. 1345.

[Spen04] K. Spencer, **The work hardening of austenitic stainless steel, applied to the fabrication of high-strength conductors**, PhD Thesis, Mc Master University, 2004.

[Tamu92] I. Tamura and C. M. Wayman, *Martensitic transformations and mechanical effects* in *Martensite*, 1992, edited by G. B. Olson and W. S. Owen for ASM, p. 227.

[Tomo86] Y. Tomota, M. Strum and J. W. Morris Jr., *Met. Trans. A*, 1986, Vol. 17A, p. 537.

[Tomo91] Y. Tomota, *ISIJ International*, 1991, Vol. 77 No. 3, p. 315.

[Varm94] S. K. Varma, J. Kalyanam, L. E. Murr and V. Srinivas, *Journal of Materials Science Letters*, 1994, Vol. 13, p. 107.

[Vena62] J. A. Venables, *Philosophical Magazine*, 1962, Vol. 7, No. 8, p. 35.

[Verc04] S. Vercammen, **Processing and tensile behaviour of TWIP steels : microstructural and textural analysis**, PhD Thesis, KUL, 2004.

[Volo76] P. Y. Volosevich, V. N. Grindnev and Y. N. Petrov, *Phys. Met. Metallogr.*, 1976, Vol 42, p. 126.

[Wu00] X. Wu and T. Y. Hsu (Xu Zuyao), *Materials Characterization*, 2000, Vol. 45, p. 137.

[Zhan02] Y. S. Zhang, X. Lu, X. Tian and Z. Qin, *Mater. Sci. Eng. A*, 2002, Vol. 334, p. 19.